HHS Public Access

Author manuscript

Nat Neurosci. Author manuscript; available in PMC 2021 March 08.

Published in final edited form as:

Nat Neurosci. 2020 September ; 23(9): 1168–1175. doi:10.1038/s41593-020-0668-9.

SPARC enables genetic manipulation of precise proportions of cells.

Jesse Isaacman-Beck[1], **Kristine C. Paik**[1,2], **Carl F. R. Wienecke**[1], **Helen H. Yang**[3], **Yvette E. Fisher**[3], **Irving E. Wang**[1,4], **Itzel G. Ishida**[5], **Gaby Maimon**[5], **Rachel I. Wilson**[3], **Thomas R. Clandinin**[1,*]

[1]Department of Neurobiology, Stanford University, Stanford, CA 94305

[2]Present address: Department of Medicine, Weill Cornell Medical College, New York, NY 10065

[3]Department of Neurobiology and Howard Hughes Medical Institute, Harvard Medical School, Boston, MA 02115

[4]Present address: Freenome, South San Francisco, CA 94080

[5]Laboratory of Integrative Brain Function and Howard Hughes Medical Institute, The Rockefeller University, New York, NY 10065

Abstract

Many experimental approaches rely on controlling gene expression in select subsets of cells within an individual animal. However, reproducibly targeting transgene expression to specific fractions of a genetically defined cell type is challenging. We developed Sparse Predictive Activity through Recombinase Competition (SPARC), a generalizable toolkit that can express any effector in precise proportions of post-mitotic cells in *Drosophila*. Using this approach, we demonstrate targeted expression of many effectors in several cell types and apply these tools to calcium imaging of individual neurons and optogenetic manipulation of sparse cell populations *in vivo*.

Introduction

Genetic labeling and manipulation of small groups of cells has provided significant insights into many aspects of biology and has been particularly impactful in studies of the nervous system. At one level, measurement and manipulation of molecularly defined cell types has become a common approach to neural circuit dissection[1]. In these approaches, cell type-specific expression of transcription factors such as Gal4[2], recombinases such as Flp[3] and Cre[4], effector proteins such as GFP[5], reporters of neuronal activity such as GCaMP[6], and optogenetic tools like channelrhodopsin[7] enables a wide range of measurements and

*Correspondence: trc@stanford.edu.

Author contributions: J.I-B., H.H.Y, I.E.W., and T.R.C conceived the study. J.I-B, C.F.R.W., H.H.Y., and Y.E.F. designed and performed the experiments under the supervision of T.R.C. and R.I.W. J.I-B., K.C.P., H.H.Y., Y.E.F., and I.G.I. generated, maintained, and/or validated transgenic fly stocks under the supervision of T.R.C, R.I.W., and G.M. J.I-B., C.F.R.W., H.H.Y., Y.E.F. and K.C.P. analyzed the data. J.I-B. and T.R.C. prepared the manuscript with contributions from C.F.R.W., H.H.Y., and Y.E.F.

Competing Interests statement: The authors declare no competing financial interests.

perturbations. Especially powerful are paradigms in which one measures the phenotypes of stochastically selected subsets of cells of the same type, because these paradigms allow assays such as single-cell characterization and within-animal comparisons between manipulated and unmanipulated cells. As a result, genetic methods to achieve such sparse manipulations are of broad interest.

A number of existing techniques can target fractions of cells of the same genetically defined cell type. In rodents, sequential recombinase-mediated switches[8,9], tamoxifen induced Cre[10], Brainbow[11], or Mosaic Analysis with Double Markers (MADM) [12] can all label subpopulations of neurons. Similarly in *Drosophila*, Mosaic Analysis with a Repressible Cell Marker (MARCM[13]), Flybow and *Drosophila* Brainbow[14,15], chemically-inducible destabilizing domains[16], and FlpOn or FlpOut approaches including MultiColor FlpOut (MCFO) [17–20] can be used to restrict effector expression. However, most of these techniques depend on limiting the spatial and/or temporal expression of a recombinase, and in both mice and flies, they require time-consuming titration of chemical or gene induction conditions. Moreover, in flies, some of these techniques depend on Gal80 suppression of Gal4 (e.g. FlpOut-Gal80[17]) and cannot be used with some commonly used cell type-selective drivers (split-Gal4[21]). Other approaches (e.g. MARCM) cannot be used in post-mitotic cells[13]. In addition, MCFO was paired with mutant recombinases with reduced activity to limit effector expression[20]. However, these recombinases may be expressed at different levels in different cell types and over time, as more recombinase is expressed, the fraction of labeled cells can change. Finally, while a wealth of refined Gal4 and split-Gal4 driver lines enable targeting of single cell types[22], selective manipulation of subsets of neurons within a driver line remains challenging. Thus, a toolkit with which one could *a priori* predict how many cells of a genetically identified type would be stochastically targeted would be of particular interest. Here we describe a technique to achieve this goal using a recombinase-dependent genetic competition with bistable outcomes whose balance can be precisely tuned by mutating recombinase target sites.

Results:

Developing a strategy for building a bistable construct.

In *Drosophila*, transgenes are often controlled by the heterologous Gal/UAS system in which the transcription factor Gal4 regulates expression of effector proteins via UAS sequences[2]. Building on this approach, we developed Sparse Predictive Activity through Recombinase Competition (SPARC) as a routine, all-genetic method for expressing effectors in defined fractions of post-mitotic cells of the same type. To do this, we generated a set of *UAS* constructs that can be switched on or off in different proportions of cells, depending on their sequences (Figure 1 and Extended Data Figure 1). We conditioned this switch on PhiC31 recombinase because it irreversibly recombines single *attP* and *attB* target sequences[23]. Furthermore, truncating canonical *attP* sequences diminishes the efficacy of recombination in *E. coli*[24], creating the possibility of tunable genetic switches.

In an initial test of this idea, we designed two constructs in which PhiC31 enables Gal4-driven expression of the calcium indicator GCaMP6f by inverting the orientation of the coding sequence (Extended Data Figure 1a,b). As a positive control, we flanked *GCaMP6f*

with canonical *attP* and *attB* sequences, while in our experimental construct, we truncated the *attP* to a 34bp sequence (*34bp_attP*) that only mediates recombination in 7% of reactions in *E. coli*[24]. We also generated transgenic flies that put expression of PhiC31 under the control of the neuronal Synaptobrevin enhancer, a construct that should lead to high levels of recombinase expression in all post-mitotic neurons (*nSyb-PhiC31*; See Figure 1, Extended Data Figure 1 and Methods for more details). To test these constructs, we used a well-defined Gal4 driver line that is active in Mi1 neurons (*Mi1-Gal4*), a population of 750 cells in each optic lobe. In *Mi1-Gal4* flies bearing *nSyb-PhiC31* and the control construct, we observed GCaMP6f expression in 100% of Mi1 cells by day 2 post eclosion (data not shown). Thus, PhiC31 can rapidly recombine *attP* and *attB* sequences in post-mitotic neurons. In contrast, using the *34bp_attP* construct, we observed GCaMP6f expression in sparse but variable fractions of neurons at day 2 post eclosion (Extended Data Figure 1c–c"). However, by day 6 post eclosion, nearly 100% of Mi1 neurons were labeled in flies bearing this *34bp_attP* construct (Extended Data 1d–d"). These results demonstrate that truncating the *attP* sequence reduces the efficiency of PhiC31 recombination *in vivo*, but in the presence of PhiC31, recombination continues to occur until every neuron is labeled. Therefore, like other sparse-labeling methods (e.g. FlpOut), using these inversion constructs would require laborious titration of the recombinase to achieve reproducible sparse labeling.

We reasoned that one way to make expression of the effector a discrete outcome would be to force PhiC31 to choose between two alternative recombination events. To do this, we designed a bistable *UAS* construct that could lead to expression of one of two effectors, Flp or LexA (Extended Data Figure 1e). Here, we set up a competition wherein PhiC31 could recombine either of two canonical *attP* sequences with a single *attB* sequence. As a result, PhiC31 will either flip the LexA coding sequence into the correct orientation for Gal4-driven expression (reaction 1) OR excise the intervening sequence, allowing for Flp recombinase expression (reaction 2). Using this construct, the outcome is discrete and irreversible because both reactions destroy the *attB* sequence. We generated flies harboring this bistable construct, *nSyb-PhiC31*, fluorescent reporters for LexA (*lexAop-myr::tdTomato*) and Flp (*UAS-FRT-stop-FRT-mCD8::GFP*[25]), and *Mi1-Gal4*. In these flies, we observed that either reaction 1 or reaction 2 happened in every Mi1 neuron by day 3 post eclosion (Extended Data Figure 1f–f"). Analogous results were observed using a pan-neuronal Gal4 (*nSyb-Gal4*[26], data not shown). As these reactions went to completion, we infer that our *nSyb-PhiC31* construct expresses sufficiently high levels of recombinase to act on the bistable switch in each neuron. However, we were surprised to note that reaction 1 and reaction 2 occurred at different relative frequencies even though two identical *attP* sequences were involved. In this construct, reaction 1 and reaction 2 are topologically distinct as one produces an inversion and the other an excision; we therefore sought a tunable cassette in which two reactions with identical topologies could result in discrete outcomes.

Tuning sparse labeling to achieve different levels of targeting.

Building on these principles, we designed SPARC, a second generation of bistable *UAS* constructs. In these constructs, two excision reactions can occur, one of which leads to effector expression and one of which does not (Figure 1a,b). In reaction 1 (Rxn 1), recombination between the first *attP* sequence and the *attB* removes a stop cassette to enable

effector expression in cells expressing Gal4 (Figure 1a,b). The reaction using the second *attP* leaves this stop sequence intact and prevents expression (Rxn 2, Figure 1a,b). Based on our inversion constructs (Extended Data Figure 1a,b), we reasoned that progressively truncating the first *attP* relative to the second *attP* would shift the equilibrium between Rxn 1 and Rxn 2 to favor retention of the stop cassette. This would tune the sparseness of effector expression by limiting expression to a smaller fraction of a cell population (Figure 1c). Based on their recombination efficiencies in *E. coli*, we generated constructs with three different *attP* variants[24] in the first position (canonical: 60bp_*attP*; truncated: 38bp_*attp* or 34bp_*attp*; Extended Data Figure 2 and see Methods for full sequences) that we predicted would target different fractions of cells (D-Dense, I-Intermediate, and S-Sparse, respectively). Taking these together, SPARC works as follows: PhiC31 expressed from *nSyb-PhiC31* rapidly recombines the SPARC construct in all neurons, and the proportion of neurons in which Rxn1 has occurred and can express effector is dictated by the *attP* variant (D, I, or S, Figure 1c). The *Gal4* expression pattern determines the selected cell type, and Gal4 successfully drives effector expression in the subset of these cells in which Rxn 1 occurred. Finally, as the recombinase reaction is stochastic and independent in each neuron, the particular subset of cells that undergo Rxn 1 or Rxn 2 will vary between animals (Figure 1c).

SPARC and SPARC2 enable effector expression at three levels.

We first tested these constructs in one of the largest genetically defined populations of neurons in the *Drosophila* optic lobe, T4 and T5 cells[27] (Figure 2a–e). In the absence of PhiC31, SPARC constructs retained the stop sequence and T4T5-Gal4 failed to drive expression of *SPARC-GCaMP6f* (Figures 1a, 2b, data not shown). When we paired the SPARC-variants with *nSyb-PhiC31*, we observed progressively fewer GCaMP6f labeled neurons from SPARC-D to SPARC-I to SPARC-S (Figure 2c–e). *SPARC-D-GCaMP6f* labeled many overlapping neurons; *SPARC-I-GCaMP6f* labeled an intermediate number of neurons; and *SPARC-S-GCaMP6f* labeled individual neurons whose dendrites could be visualized (Figure 2e, inset). We observed similar results in Kenyon cells, lobula columnar neurons, and several columnar neurons in the optic lobe (Extended Data Figure 3 and data not shown). These data are consistent with the notion that SPARC variants can determine the fraction of cells that express effector across cell types and animals.

To generalize the SPARC technique, we next made *SPARC-LexA::p65* transgenes. LexA::p65 is a transcription factor that drives expression of transgenes under the control of the lexAop promoter[28]; this system is orthogonal to the Gal4/UAS expression system[29]. Using *SPARC-LexA::p65* in the absence of PhiC31 recombinase, 100% of neurons expressed LexA::p65, as assayed using *lexAop-myr::tdTomato*. (Figure 2g–g”). This result suggested that the widely-used stop cassette[28] that we used in the initial SPARC design (Fig. 1a) might permit a low level of read-through that can be detected by sensitive outputs like LexA::p65 (and mCD8::GFP, data not shown).

To avoid this read-through, we generated SPARC2, in which we incorporated two self-cleaving ribozymes from the hepatitis delta virus (HDV) into the SPARC module (Figure 2f). We reasoned that these self-cleaving ribozymes should truncate any read-through transcript prior to translation[30,31]. We first examined *SPARC2-LexA::p65* transgenes in Mi1

neurons in the absence of PhiC31 and observed a 10,000-fold decrease in read-through (~0.01% of Mi1 cells labeled with myr::tdTomato, Figure 2h–h", data not shown). Importantly, in the presence of PhiC31, the D, I, and S variants of *SPARC2-LexA::p65* behaved qualitatively similarly to the corresponding *SPARC-GCaMP6f* transgenes (Figure 2i–k"). Thus, HDV ribozymes effectively eliminate read-through and enable SPARC2 transgenes to express both direct and amplifying effectors in three different proportions of cells.

Quantitative validation of SPARC2 efficacy across cell types.

Our goal was to build a toolkit that could predictively target desired fractions of individual neurons within any population. In the *Drosophila* brain, identified neuronal populations vary widely in number. For example, in the visual system, there are approximately 6000 T4 and T5 neurons per optic lobe[27] but only three HS neurons[32]. We first determined whether the three SPARC2 variants (D, I, S) allow targeting of different fractions of individual neurons across animals and cell types by generating *SPARC2-mCD8::GFP* transgenes and observing SPARC2-labeling at all three levels in five different neuronal populations: T4 and T5 (~6000 cells per optic lobe[27]; Figure 3a–c), Mi1 (~750 cells per optic lobe[33], Figure 3d–f), GH146+ olfactory projection neurons (PNs, ~91 cells per antenna lobe[34]; Figure 3g–i), LC20 (~29 cells per optic lobe[35]; Figure 3j–l;), and HS (3 neurons per optic lobe[32]; m-o). To quantify how precise the SPARC2-variants are at targeting specific fractions of cells across different animals and distinct cell types, we co-labeled all Gal4 expressing cells with UAS-driven myr::tdTomato and quantified the mCD8::GFP labeled neurons as a percentage of the total population (Figure 3p–r). Remarkably, for each SPARC2 variant, mCD8::GFP was expressed in a similar percentage of neurons across cell types. *SPARC2-D-mCD8::GFP* labeled ~48–51% of cells, *SPARC2-I-mCD8::GFP* labeled ~17–22% of cells, and *SPARC2-S-mCD8::GFP* labeled ~3–7% of cells (Figure 3p–r).

A common experimental goal is to selectively label individual cells within a population. Impressively, despite cell numbers that span more than three orders of magnitude, we were able to reliably label individual cells in each population with at least one of the three SPARC2 variants. We labelled individual T4 and T5 dendrites with SPARC2-S (Figure 3c). For Mi1, SPARC2-I labeled the most non-overlapping cells (Figure 3e), though SPARC2-S also labeled individual neurons (Figure 3f). SPARC2-I and SPARC2-S were similarly effective in labeling individual GH146+ olfactory PNs (Figure 3h,i) or LC20 neurons (Figure 3k,l), while both SPARC2-D and SPARC2-I routinely labeled individual HS neurons (Figure 3m,n,p,q). As this set of cell types spans the full range of variation in neuron population size in the *Drosophila* brain, these data demonstrate that single cell isolation can now be routine using the SPARC2 toolkit.

SPARC and SPARC2 effector expression are stochastic.

To determine whether SPARC2 labeled stochastically distributed subsets of neurons across animals, we took advantage of the *GH146-Gal4* pattern that targets approximately 91 olfactory PNs in every animal[34] (Figure 4a–g'). These PNs innervate distinct glomeruli in the antenna lobe, making it easy to determine whether distinct subsets of neurons are labeled in different animals. Consistent with the stochastic nature of PhiC31 recombination, we

observed different patterns of PN labeling in every *SPARC2-I-mCD8::GFP* and *SPARC2-S-mCD8::GFP* animal (n=10 each, Figure 4 and data not shown). We observed similar results using other Gal4 drivers and SPARC and SPARC2 effectors (data not shown). In summary, these data demonstrate that the SPARC and SPARC2 toolkit reliably labels precise proportions of neurons that are stochastically distributed and can be revealed with any Gal4 driver.

SPARC and SPARC2 enable facile neural circuit measurement and perturbation.

To investigate the functional utility of SPARC, we used SPARC-S-GCaMP6f to image calcium (Ca^{2+}) responses in the dendrites of individual T5 neurons. These neurons preferentially respond to visual motion in one direction, a direction selectivity that is first observed in their dendrites[36,37]. As the dendrites of individual T5 neurons lie in close physical proximity and can have different direction selectivities, labeling individual cells is critical to measuring their functional properties. Previous attempts to image from individual T5 cells relied on laborious FlpOut approaches that required titrated and temporally precise heat shocks of *Drosophila* larvae to restrict effector expression to a subset of cells[37–39]. In contrast, the SPARC method consistently labeled fewer T5 neurons that were more distributed throughout the *T4T5-Gal4+* population, than the sparsest FlpOut labeling we could achieve using a brief and developmentally late heat-shock (Figure 5a,b). More importantly, when we imaged visually evoked Ca^{2+} responses in regions of interest (ROIs) representing T5 dendrites, we observed that the fluorescent signals from SPARC-labeled ROIs were significantly more direction selective than those from FlpOut-labeled ROIs (DSI; Figure 5c–e). This result reflects the fact that SPARC labeling was sparser than the sparsest FlpOut labeling we could achieve. As a consequence, SPARC ROIs more cleanly captured signals from single cells, while FlpOut ROIs likely included signals from multiple labeled cells with different directional preferences (see Methods). Thus, both anatomical and functional evidence suggests that SPARC isolates single T5 dendrites more easily and more consistently than standard FlpOut approaches.

To determine if we could use this approach to manipulate the activity of neuronal subpopulations, we generated *SPARC2-CsChrimson::tdTomato* transgenic flies[40]. We expressed this construct in ring (R) neurons, GABAergic neurons that send sensory input to the central complex[41]. R neurons are divided into types based on morphology[42]; here we focused on the R2 type. We expressed SPARC2-D-CsChrimson::tdTomato in a subset of R2 neurons (Figure 6a–c") and performed whole-cell recordings from $tdTomato^{+}$ and $tdTomato^{-}$ R2 neurons. We observed that $tdTomato^{+}$ R2 neurons were depolarized by light, while $tdTomato^{-}$ R2 neurons were not depolarized (Figure 6d,e). Indeed, $tdTomato^{-}$ R2 neurons were slightly hyperpolarized by light, implying that these R2 neurons were inhibited by other R2 neurons that express CsChrimson. Thus, *SPARC2-CsChrimson* allows optogenetic activation of sparse cell populations within a single cell type, enabling the discovery of interactions among them, such as mutual inhibition.

Discussion:

The existing SPARC and SPARC2 toolkit.

The SPARC and SPARC2 toolkit provides facile manipulation of three precise proportions of any cell type. We include direct effector transgenes that can be used to label cells (mCD8::GFP), to observe changes in intracellular calcium concentration (GCaMP6f, jGCaMP7f) and membrane potential (ASAP2f), as well as to optogenetically modulate neuronal activity (CsChrimson). In addition, the availability of the indirect effector transgene *SPARC2-LexA::p65* opens the possibility of sparsely expressing a large range of additional existing effectors under the control of *lexAop* (Extended Data Figure 4). To provide the flexibility to target both neuronal and non-neuronal cells, we also generated transgenic animals that express PhiC31 pan-neuronally (*nSyb-PhiC31*), ubiquitously (*tub-PhiC31*), and in any cell type expressing Gal4 (*UAS-PhiC31*). As a result, we think that this toolkit will be broadly applicable in its current form.

Comparisons with other methods.

Extant approaches to label precise proportions of cells required user titration of recombinase expression levels or activity. For SPARC and SPARC2, we bypass this effort through a construct that is designed to utilize a strong, saturating source of PhiC31 recombinase. To perform a diverse array of experiments on single cells or on precise proportions of cells of a given genetically defined type, one can simply generate flies with the appropriate combination of transgenes (Figures 1–4; see Methods and Extended Data Figure 4 for example crosses and restrictions on stock maintenance). Alternatively, if additional tuning of recombinase levels is required, one can use other PhiC31 sources, including the *UAS-PhiC31* transgene that we provide. Furthermore, unlike previous methods of sparse manipulation that depend on cell division (MARCM, MADM), SPARC and SPARC2 can circumvent development to specifically manipulate post-mitotic neurons. Finally, SPARC and SPARC2 can be easily paired with split-Gal4 drivers to label and manipulate very precisely defined cell populations.

Future modification and potential use cases of SPARC2.

To ensure that any user can easily incorporate any current or future genetically encoded effector into this toolkit, we designed each element to be modular and easily manipulated (Extended Data Figure 2, Methods). For example if one wanted to target other precise proportions of cells, one could explore further mutagenesis of SPARC2's *attP* or *attB* target sites[24], or one could exchange the position of the truncated *attP* and canonical *attP* within the SPARC2 cassette (which should enable effector expression in >50% of cells). Moreover, in addition to *nSyb-PhiC31*, the toolkit includes *UAS-PhiC31* and *tub-PhiC31* constructs and transgenic animals to alter where and when PhiC31 is expressed. In the context of the nervous system, SPARC, SPARC2, and future variations will allow convenient and unparalleled access to define single neuron contributions to neural circuit processing. By making single cell measurements and perturbations routine, we enable precise characterization of single neuron properties. In non-neuronal cells, SPARC will enable wide-ranging studies that exploit mosaic analysis to investigate cell biology and physiology.

Finally, as PhiC31 functions in both the mouse and fish[43,44], we anticipate that this strategy will be widely generalizable to other model systems.

Methods

Generation of plasmids for transgenesis:

All plasmids were generated with In-Fusion cloning (Takara Biotech; Mountain View, CA, USA) using the primers described in Supplementary Table 1 or were generated through synthesis and molecular cloning by Genscript (Piscataway, NJ, USA). Constructs were sequence-verified by single primer extension (Sequetech; Mountain View, CA, USA). We have submitted the constructs from Supplementary Table 2 to Addgene. All other constructs are available upon written request.

PhiC31 recombinase construct synthesis:

We generated three constructs to express PhiC31 recombinase under the control of different promoters: 20XUAS, Tubulin (tub), and neuronal Synaptobrevin (nSyb). These constructs were built in the backbone of pJFRC7 (Addgene #26220) [28]. To generate pJFRC-20XUAS-IVS-PhiC31, we PCR-amplified a Kozak consensus sequence followed by the PhiC31 recombinase open reading frame and an NLS sequence from vector pBS130[46] and cloned it into the backbone via XhoI and XbaI sites. To generate pJFRC-αTub84B-IVS-PhiC31, we PCR-amplified the Tubulin 1 alpha (αTub84B) promoter from pIDT-attB-Tub_NLSGal4DBDlink-PBT[46] and replaced the 20XUAS promoter in pJFRC-20XUAS-IVS-PhiC31 by cloning into the HindIII and BglII sites. To generate pJFRC-nSyb-IVS-PhiC31, the nSyb promoter was PCR-amplified from the pattB-synaptobrevin-4-QFBDMD-G4AD-hsp70 plasmid (Addgene #46112) [26] and cloned into the pJFRC-αTub84B-IVS-PhiC31 backbone via BglII sites flanking the αTub84B promoter. We submitted the pJFRC-nSyb-IVS-PhiC31 plasmid to Addgene (see Supplemental Table 1).

Synthesis of SPARC development, SPARC and SPARC2 CRISPR donor plasmids:

To generate the CRISPR donor backbone plasmid, pHD-3xP3-dsRed-ΔattP, we used site-directed mutagenesis (Quikchange, Stratagene XL; Agilent, Santa Clara, CA, USA) to replace the *attP* sequence in the CRISPR donor vector pHD-AttP-3XP3-dsRed[47] with unique KpnI and MluI restriction enzyme sites using primer pair 1 (Supplemental Table 1). To target the *attP40* region of the genome, we PCR-amplified a 1040 base pair (bp) left homology arm (2L:5106650..5107689) and an 1168bp right homology arm (2L:5108423..5109590) from genomic DNA from the IsoD1 *Drosophila* strain[48]. These left and right homology arms were first cloned into PCR2.1d-topo (Invitrogen, Waltham, MA, USA) using primer pairs 2 and 4 (Supplementary Table 3) and were then subcloned into pHD-3XP3-dsRed-ΔattP using primer pair 3 via NotI and primer pair 5 via SapI, respectively. Primer pairs 3 and 5 added external flanking guide RNA (gRNA) target sites to enable Cas9-mediated linearization of the donor sequence *in vivo* (see Extended Data Figure 2, Supplementary Table 2).

Next, several SPARC development, SPARC, and SPARC2 cassettes were synthesized by Genscript (Piscataway, NJ, USA) and cloned into the unique KpnI site (Extended Data

Figure 2, Supplementary Table 3). We then swapped effectors in these SPARC and SPARC2 Donor plasmids via In-Fusion cloning with SalI restriction digest (Clontech, Mountain View, CA, USA) or using the CloneEZ method (Genscript, Piscataway, NJ, USA). Each SPARC and SPARC2 construct contains 2 *attP* sequences and 1 *attB* sequence; we used sequences previously defined in[24]. The first *attP* has a variable sequence depending on the SPARC or SPARC2 variant (D, I, S; Fig. 1a, Extended Data Figure 1). Below we list these sequences and how they are used in each SPARC or SPARC2 variant:

60bp_attP Sequence (D variant):
CGGGAGTAGTGCCCCAACTGGGGTAACCTTTGAGTTCTCTCAGTTGGGGGCGTAG GGTCG

38bp_attP Sequence (I variant):
CCCCAACTGGGGTAACCTTTGAGTTCTCTCAGTTGGGG

34bp_attP Sequence (S variant): CCAACTGGGGTAACCTTTGAGTTCTCTCAGTTGG

70bp_attB Sequence:
CTCGAAGCCGCGGTGCGGGTGCCAGGGCGTGCCCTTGGGCTCCCCGGGCGCGTA CTCCACCTCACCCATC

For detailed construct maps of SPARC and SPARC2 as well as recommended methods for modular swapping of the effector, see Extended Data Figure 2.

gRNA-targeting vector logic and synthesis:

We defined gRNA targets for insertion around the *attP40* region of the genome using the publicly available search tool: flybase.org/crispr/[49]. The sequence and genomic location of these target sites as well as the synthetic gRNA used for donor plasmid linearization are described in Supplementary Table 4. We validated that these near-attP40 gRNA targets were present and unmutated in our CRISPR target flies (*y sc v; +* ; *P{Nos-Cas9}attP2*, TH00787; kind gift from Norbert Perrimon) by PCR amplification and sequencing. Finally, we generated the construct pCFD5-attP40-gRNA using previously described methods (http://www.crisprflydesign.org/plasmids/) by PCR-amplifying the three gRNA components and inserting them into the pCFD5: U6:3-t::gRNA backbone (a gift from Simon Bullock, Addgene #73914) via Bbs-I. Two of these gRNAs targeted neighboring genomic regions near the attP40 genomic locus in our CRISPR-HDR target flies. We added a third gRNA component that targeted the synthetic gRNA sequence that flanks the donor insertion sequence in our pHD donor vectors (Extended Data Figure 2). This synthetic gRNA has no predicted off-target recognition in the *Drosophila melanogaster* genome.

Generation of transgenic flies:

All PhiC31-expressing transgenic flies were generated using site-specific insertion into the genome (Bestgene; Chino Hills, CA, USA). These transgenes carry the mini-*white* marker; their genomic locations are listed in Supplementary Table 5.

SPARC transgenic flies were generated by Bestgene (Chino Hills, CA, USA) via standard construct injections (100–500ng donor construct, 75–250ng gRNA construct) and CRISPR-HDR. Transformants were identified by expression of the marker 3xP3-DsRed which was later excised from the genome using Cre recombinase as previously described[47]. We maintained ≥3 independent isolates for each transgene and tested them for expression and function.

Genomic insertion site validation:

To validate the insertion SPARC transgenes near the *attP40* locus, we PCR amplified genomic DNA with primer pairs in which one primer recognizes a genomic sequence outside of the homology arm and the other recognizes a sequence within the transgene. For every SPARC or SPARC2 transgenic fly, we ensured amplification of a PCR product from both the 5' and 3' sides of the transgene. The primer pairs and expected product sizes are in Supplementary Table 6. All transgenic insertions were validated by PCR with the exception of *TI{20XUAS-SPARC-D-Chrimson::tdTomato-3.1}CR-P40*. This transgene is missing ~300bp of the left homology arm. However, we validated the function of this transgene in Figure 6.

Complete Fly Stock List, Fly Genotypes, Origin of Transgenes:

A list of all transgenic flies generated in this study can be found in Supplementary Table 5. Fly genotyes (by figure) and origin of transgenes are listed in Supplementary Information.

Fly Husbandry:

All flies were raised on molasses-based food at 25°C with the exception of CsChrimson-expressing flies, which were raised on Nutri-Fly German Food (#66–115, Genesee Scientific, San Diego, CA, USA) food containing all-trans-retinal (0.6mM). Conditions for specific experiments are described below.

Brain Dissection, Immunolabeling and Confocal imaging:

Note: brain dissection, immunolabeling, and confocal imaging were performed in two different laboratories with slightly different protocols.

For Figures 2–4, Extended Data Figures 1, 3 (Clandinin laboratory):

Brain dissections were performed on 4–6 day old adult female flies. Flies were ordered in a fly collar, the proboscis and antennae were removed for each fly and flies were perfused with freshly-made 2% PFA in Phosphate-Buffered Lysine for 50min. We removed the fixative and washed brains 3X with ice-cold PBS and then proceeded to extract brains with fine forceps. Brains were stored in ice cold PBS + 0.1% Triton-X (PBS-Tx) for up to 2 hours and then were moved to a PBS-Tx + 10% Normal Goat Serum (NGS) blocking solution for 30min at room temperature. We incubated the brains in the following primary antibodies for 3 days at 4°C: anti-GFP (chicken, Abcam, Cambridge, UK, GB 1:2000), anti-Bruchpilot (nc82, mouse, Developmental Studies Hybridoma Bank, Iowa City, IA, USA 1:30), anti-DsRed (rabbit, Takara Bio, Mountain View, CA, USA, 1:700). The anti-GFP antibody recognized both GFP and GCaMP6f. The anti-DsRed recognized myr::tdTomato. After

primary incubation, brains were washed 3 × 15min in PBS + 0.1% Triton-X and then subjected to secondary staining for 2hrs at room temperature. All secondary antibodies were diluted 1:200 in PBS-Tx + NGS; these included anti-chicken Alexa 488 (Life Technologies, Carlsbad, CA, USA), anti-rabbit-Cy3 (Life Technologies, Carlsbad, CA, USA), and anti-mouse Alexa 633 (Life Technologies, Carlsbad, CA, USA). Brains were then washed 3 × 15min in PBS + 0.1% Triton-X, incubated for at least 1hr in 70% glycerol for tissue clearing and mounted individually on glass slides in Vectashield (H-1000, Vector Laboratories, Burlingame, CA, USA) for confocal imaging.

Brains were imaged on a Leica SP8 confocal microscope. Series of between 20 and 100 optical sections (1–5μm spacing; total 20–200μm) were imaged using either a Leica HC PL APO 20x/0.70 CORR CS oil-immersion lens (N.A. 1.3) or a Leica HC PL APO 40x/1.30 CS2 40x oil-immersion lens (N.A. 1.42). Tiffs of single confocal planes or maximum intensity projections (MIPs) were made in Imaris 9.3 (Oxford Instruments, Abingdon, UK, GB). For Figure 2 and Figure 3a–f, MIPs were from 3 × 3μm sections (9μm) of tissue. For Figure 3g–I and Figure 4, MIPs were from ~15 × 2μm sections (30μm) of tissue. For Figure 3j–o, MIPs were from 15–20 × 3μm sections (45–60μm) of tissue. For Extended Data Figure 3a–d, MIPs of Mushroom Bodies were generated from 15–20 5μm optical sections, while images of cell bodies (Kenyon cells, Extended Data Figure 3e–h") were taken from single optical sections.

Image Processing:

Tiffs of single confocal planes or MIPs were generated in Imaris 9.3 (Oxford Instruments, Abingdon, UK, GB) and subsequently rotated and cropped to the same dimensions using Adobe Photoshop (Adobe, San Jose, CA, USA). Brightness levels were uniformly adjusted in Adobe Photoshop across images that were compared within a figure.

Cell Counting (Figure 3):

For all T4 and T5 samples and SPARC2-D and SPARC2-I labeled Mi1 samples, cell bodies were imaged at 40X using a series of 10–12 optical sections spaced 1μm apart as described above. Subsequently, single planes from the top, middle, and bottom of these stacks were isolated for each optic lobe (n = 10 per condition) and individual tiffs were generated for myr::tdTomato and mCD8::GFP stains from these planes. We randomly shuffled these images and a blinded author manually counted the individual cell bodies in each channel in Adobe Photoshop. For SPARC2-S labeled Mi1 cells, GH146-Gal4+ olfactory PNs, LC20 neurons, and HS neurons, optical sections were taken through the full extent of Gal4 labeled cells 1–3μm apart. Single color 3D projections were generated in Imaris for all samples and ALL myr::tdTomato+ or mCD8::GFP cell bodies were counted separately. We calculated the percent of SPARC-labeled cells as total number of SPARC-labeled cells/total number of cells labeled in the Gal4 pattern by myr::tdTomato. We first used 1-way ANOVA to determine whether there were statistically significant differences between the proportion of mCD8::GFP labeled cells for each SPARC2 variant by cell type and for each cell type by SPARC2 variant. When significant differences were detected, we used pairwise two-tailed Student's t tests to define statistical differences within groups. We excluded HS from

statistical analyses as there are only 3 cells in this population, and we would not expect a normal distribution when labeling ~50%, ~20%, or ~5% of cells in such a small population.

For Figure 6 (Wilson laboratory):

For immunostaining brain dissections, newly eclosed female flies that were raised on 0.6 mM all-trans-retinal-containing Nutri-Fly German Food (#66–115, Genesee Scientific, San Diego, CA, USA) were collected on CO_2. The brains were then dissected out of the head in chilled external saline[50]. Immunostaining was then performed as follows. Brains were (1) fixed in 4% paraformaldehyde (15714, Electron Microscopy Sciences, Hatfield, PA, USA) in phosphate buffered saline (PBS; 46–013-CM, Thermo Fisher Scientific, Waltham, MA, USA) for 15 minutes at room temperature; (2) washed 3 times for 15 min with PBST (PBS with 0.44% Triton X-100 (T-8787, Sigma-Aldrich, St. Louis, MO, USA)); (3) incubated in a blocking solution of 5% normal goat serum (NGS; G9023, Sigma-Aldrich, St. Louis, MO, USA) in PBST for 20 min; (4) incubated in a primary antibody solution containing mouse anti-Bruchpilot antibody (1:25, nc82, Developmental Studies Hybridoma Bank, Iowa City, IA, USA), chicken anti-GFP (1:1000, ab13970, Abcam, Cambridge, UK, GB), and rabbit anti-dsRed (1:500, 632496, Takara Bio, Mountain View, CA, USA) diluted in the NGS blocking buffer for 48 hr at room temperature on a rotating nutator; (5) washed 3 times for 15 min with PBST; (6) incubated in a secondary antibody solution containing Alexa 488-conjugated goat anti-chicken (1:250, A-11039, Thermo Fisher Scientific, Waltham, MA, USA), Alexa 568-conjugated goat anti-rabbit (1:250, A-11011, Thermo Fisher Scientific, Waltham, MA, USA), and Alexa 633-conjugated goat anti-mouse (1:250, A-21050, Thermo Fisher Scientific, Waltham, MA, USA) in blocking solution for 24 hr at room temperature on a rotating nutator; and (7) washed 3 times for 15 min with PBST.

Brains were mounted on slides in Vectashield (H-1000, Vector Laboratories, Burlingame, CA, USA) in the anterior-posterior orientation and then imaged using a Leica SPE confocal microscope. Series of between 30 and 100 optical sections (1.0 μm spacing) were imaged using either an Olympus UPLFLN 40x oil-immersion lens (N.A. 1.3) or an Olympus PLAPON 60x oil-immersion lens (N.A. 1.42). MIPs of the cell body images were made in Fiji[51], and MIPs of the full R2 neuron morphology were made in Imaris 9.3 (Oxford Instruments, Abingdon, UK, GB).

Fly preparation for 2-photon imaging:

For two-photon imaging of T5, we used the enhancer fragment VT025965 to drive expression of Gal4 in T5 with high specificity[52]. Sparse expression of GCaMP6f was achieved using either a FlpOut or SPARC strategy. For the FlpOut strategy, we used the genotype *+/y w, P{hsFLP}; P{20XUAS-IVS-GCaMP6f}attP40/ P{αtubP(FRT.stop)Gal80}2; P{VT025965-Gal4}attP2/+.* We heat-shocked at 37°C for 90 seconds during the late 3rd instar stage of development[37]. This heat shock protocol yielded the sparsest expression pattern for this T5 driver. Shorter or developmentally later heat shock resulted in either no GCaMP6f expression, or no observable GCaMP6f signals. For the SPARC strategy, we used the genotype *+; TI{20XUAS-SPARC-S-GCaMP6f}CR-P40 / P{nSyb-IVS-PhiC31}su(Hw)attP5; P{VT025965-Gal4}attP2/ +.*

All flies were female, and were imaged within 5–7 days of eclosion. Flies were immobilized by chilling on ice, and affixed to a custom-built mount with UV-cured optical epoxy (NOA 63, Norland Products, Cranbury, NJ, USA). The cuticle, fat bodies, and trachea of the left hemisphere were removed under ice-cold, artificial hemolymph without calcium[50] to expose the brain for imaging from above. During imaging, standard, carbogen-gassed, room-temperature artificial hemolymph[50] was perfused across the brain at 150 mL/h.

Imaging and delivery of visual stimuli:

Imaging and delivery of visual stimuli followed Leong et al. 2016[38]. Fluorescence was monitored *in vivo* using two-photon microscopy. We used a Leica SP 5 II equipped with the HCX APO L 20X/NA1.00 water dipping lens (Leica, Wetzlar, Germany). GCaMP6f was excited at 920 nm, and the power was ~5–8 mW at the stage. Recordings lasted ~3.5 minutes. GCaMP6f fluorescence signals were acquired with a bandpass filter (525/50m), at ~20 Hz (bidirectional scanning at 1.4 kHz, across a FOV of 128 pixels x 256 pixels, rows x columns). Pixels measured ~290 x ~290 nm. The stimulus screen subtended ~ 60° x 90° (azimuth x elevation) of the left visual field. Visual stimuli were delivered with a LightCrafter 4500 DLP (Texas Instruments, Dallas, TX, USA) using a 100 Hz frame rate. The LightCrafter was configured to use only the blue LED, then the stimulus was filtered with a 447/60 bandpass filter (Semrock, IDEX Health and Science, Rochester, NY, USA), and a ND1 filter (Thorlabs, Newton, NJ, USA). The mean radiance was ~0.04 W sr^{-1} m^{-2}.

Identification and selection of ROIs:

ROI selection involved two stages: (1) automated segmentation[53] of GCaMP6f responses to moving sinusoidal gratings to obtain an initial set of ROIs, each representing approximately individual cells, and (2) exclusion of ROIs from this initial set if they did not match the known calcium response properties of T5[37,38], or if their spatiotemporal receptive fields did not lie in the center of the stimulus screen, yielding a final set of ROIs that best represent individual T5 dendritic arbors. As T5 dendrites are fine and interdigitating, this ROI selection strategy could not always isolate dendritic arbors of individual T5 cells, particularly for FlpOut clones, since the sparsest possible FlpOut expression pattern that we could achieve was denser than the sparsest possible SPARC expression pattern. GCaMP6f responses to moving light and dark edges were used to confirm dark contrast selectivity (data not shown), and the timing of responses to moving dark edges was used to determine whether the cell's spatiotemporal receptive field was centered on the stimulus screen (data not shown). Two ROIs that did not meet these criteria were not further analyzed and were excluded.

Stimulus design and data analysis for T5 calcium imaging experiments:

We presented sinusoidal gratings (1Hz, 25°/cycle, 100% contrast) moving for 5 seconds in 8 equally-spaced directions. Each 5-second bout was preceded by a 3-second "blank" (a gray screen of luminance matching the mean luminance of the gratings). We presented 3 complete cycles of all 8 directions, in a random order, for a total recording duration of ~3.5 minutes.

GCaMP6f fluorescence responses were quantified as the average $\Delta F/F_0$ across pixels within each ROI, where F_0 was defined as the mean fluorescence within each ROI during the final 5 frames of the "blank" preceding each bout. Responses were averaged across all three bouts to obtain the mean response to each direction of motion (plotted in Figure 5c). Tuning curves (Figure 5d) were derived from these mean responses, plotted as the maximum $\Delta F/F_0$ for each direction, normalized by the maximum $\Delta F/F_0$ across directions (the PD response), and registered across ROIs to align the PD response before averaging across ROIs. For each ROI, the DSI (Figure 5e) was calculated as the vector average of response amplitudes to the 8 directions of motion, normalized by the sum of response amplitudes to all 8 directions of motion.

Flies with zero ROIs meeting selection criteria (Methods), or with no visually responsive ROIs, were excluded from further analysis (zero SPARC flies, two FlpOut flies). These exclusion criteria were pre-determined.

Fly preparation and dissection for electrophysiology:

Newly eclosed virgin female flies were collected on ice approximately 1–4 hrs before the experiment. All flies were raised on 0.6 mM all-*trans*-retinal-containing Nutri-Fly German Food (#66–115, Genesee Scientific, San Diego, CA, USA) and fly vials were wrapped in foil to prevent photo-conversion of the all-trans-retinal. At the beginning of each dissection, the fly was cold-anesthetized.

The preparation holder consisted of a flat titanium foil secured in an acrylic platform, with the foil oriented parallel to the horizontal body plane; the fly's head and body were gently pushed partway-through a hole in the foil. The head was pitched backward so that the anterior surface was oriented dorsally in the holder. The fly was always secured in the holder with epoxy (Loctite AA 3972, Hartford, CT, USA) cured using a brief (<1s) pulse of UV light (LED-200, Electro-Lite Co, Danbury, CT, USA). After the dorsal portion of the head was covered in saline, a large hole was cut in the head capsule and the retina and trachea on one side of the brain were removed to expose the neurons of interest. To reduce brain movement, muscle 16 was severed, and the proboscis was removed. An aperture was made in the perineural sheath around the somata of interest by ripping gently with fine forceps.

The external solution contained (in mM): 103 NaCl, 3 KCl, 5 N-tris(hydroxymethyl) methyl-2-aminoethane-sulfonic acid, 8 trehalose, 10 glucose, 26 $NaHCO_3$, 1 NaH_2PO_4, 1.5 $CaCl_2$ and 4 $MgCl_2$, with osmolarity adjusted to 270–273 mOsm. External solution was bubbled with 95% O_2 and 5% CO_2 and reached a final pH of 7.3. External solution was continuously perfused over the brain during electrophysiology.

Whole-cell patch clamp recordings:

In vivo whole-cell patch clamp recordings were performed as described previously[54]. Patch pipettes were made from borosilicate glass (1.5mm O.D., 0.86 I.D., # BF150-86-7.5HP, Sutter Instrument Co., Novato, CA, USA) using a Sutter Instrument Co. P-97 puller. Pipettes resistance ranged from 5–12 MΩ. The internal solution contained (in mM): 140 potassium aspartate, 10 4-(2-hydroxyethyl)-1-piperazineethanesulfonic acid, 4 MgATP, 0.5 Na_3GTP, 1

ethylene glycol tetraacetic acid, 1 KCl, and 13 biocytin hydrazide. The pH was 7.3, and the osmolarity was adjusted to ~268 mOsm. Recordings were performed at room temperature.

To obtain patch-clamp recordings under visual control, we used an Olympus BX51WI microscope with a 40X water-immersion objective (LUMPlan FI/IR NA 0.8, Olympus, Shinjuku City, Tokyo, Japan). GFP and tdTomato expressing neurons were identified using an Hg-lamp source (U-LH100HG, Olympus, Shinjuku City, Tokyo, Japan) with an EGFP-longpass filter (U-N41012, Chroma, Bellows Falls, CT, USA) or a TRITC-Cy3 filter (Chroma, Bellows Falls, CT, USA).

To visualize the brain for recordings, far-red light was delivered from a fiber-coupled LED (740nm, M740F2, Thorlabs, Newton, NJ, USA) via a ferrule patch cable (200 μm core, Thorlabs, Newton, NJ, USA) plugged into a fiber optic cannula (Ø1.25 mm SS ferrule 200 μm core, 0.22 NA, Thorlabs, Newton, NJ, USA) glued to the recording platform, with the tip of the cannula ~1 cm behind the fly.

Recordings were obtained using an Axopatch 200B amplifier and a CV-203BU head-stage (Molecular Devices, San Jose, CA, USA). Voltage signals were low-pass filtered at 5 kHz prior to digitization and then acquired with a NiDAQ PCI-6251 (National Instruments, Austin, TX, USA) at 20 kHz. Liquid junction potential correction was performed *post hoc* by subtracting 13 mV from recorded voltages[55]. When a stable whole-cell recording was achieved, the initial resting membrane potential was measured. Consistent with what one might expect from expression of a cation channel, we observed differences in the resting membrane potential and input resistance between cells expressing CsChrimson and control cells (described in Supplementary Table 7). During optogenetic stimulation, a constant hyperpolarizing current was applied to bring the cell's membrane potential to between −50 mV and −60 mV.

For optogenetic stimulation, the Hg-lamp source (U-LH100HG) was used to deliver a 50-ms pulse of green light (530–550 nm, 2–4 mW, TRITC-Cy3 filter cube, Chroma, Bellows Falls, CT, USA) via the objective. A shutter (Uniblitz Electronic, Rochester, NY, USA) controlled the pulse duration.

Electrophysiology data analysis and data inclusion:

To measure CsChrimson-evoked responses, the mean of 10 replicate stimulation trials was taken and filtered using a median filter with a 20-ms window to remove the effect of spiking activity. Evoked response amplitudes were the largest deviation from baseline that occurred within the 500 ms following the optogenetic stimulation. The one second preceding stimulation was used as the measurement of baseline membrane voltage.

Cells were only analyzed if the resting membrane voltage of the cell was < −30mV immediately following break in. One of eight recordings were excluded based on this criterion.

Statistics:

The following statistical tests were used in this study: 1) One way ANOVA (Figure 3p–r) and 2) two-tailed student's t-test (Figures. 3r, 5e, Extended Data Figure 2). No statistical methods were used to pre-determine sample sizes but our sample sizes are similar to those reported in previous publications[39,55,56]. Data distribution was assumed to be normal for all experiments except for quantification of HS cell labeling (Figure 3p–r). These HS cell data were excluded from statistical comparisons as described above.

Randomization and Blinding:

Stimulus presentation was randomized for the experiments in Figure 5. Otherwise, data collection was not randomized. Cell counting for Figure 3 was done by a blinded observer, but otherwise data collection and analysis were not performed blind to the conditions.

Note: More detailed information on statistics, data exclusions, randomization and blinding, and reagents can be found in the Life Sciences Reporting Summary associated with this paper.

Code availability

All analysis was carried-out using custom-written MATLAB code https://github.com/wienecke/SPARC. Visual stimuli were programmed with the OpenGL 1.0 API in Visual C#. All code is available on Github and will be made available upon request from the corresponding author.

Data availability:

The data that support the findings of this study are available from the corresponding author upon request.

Extended Data

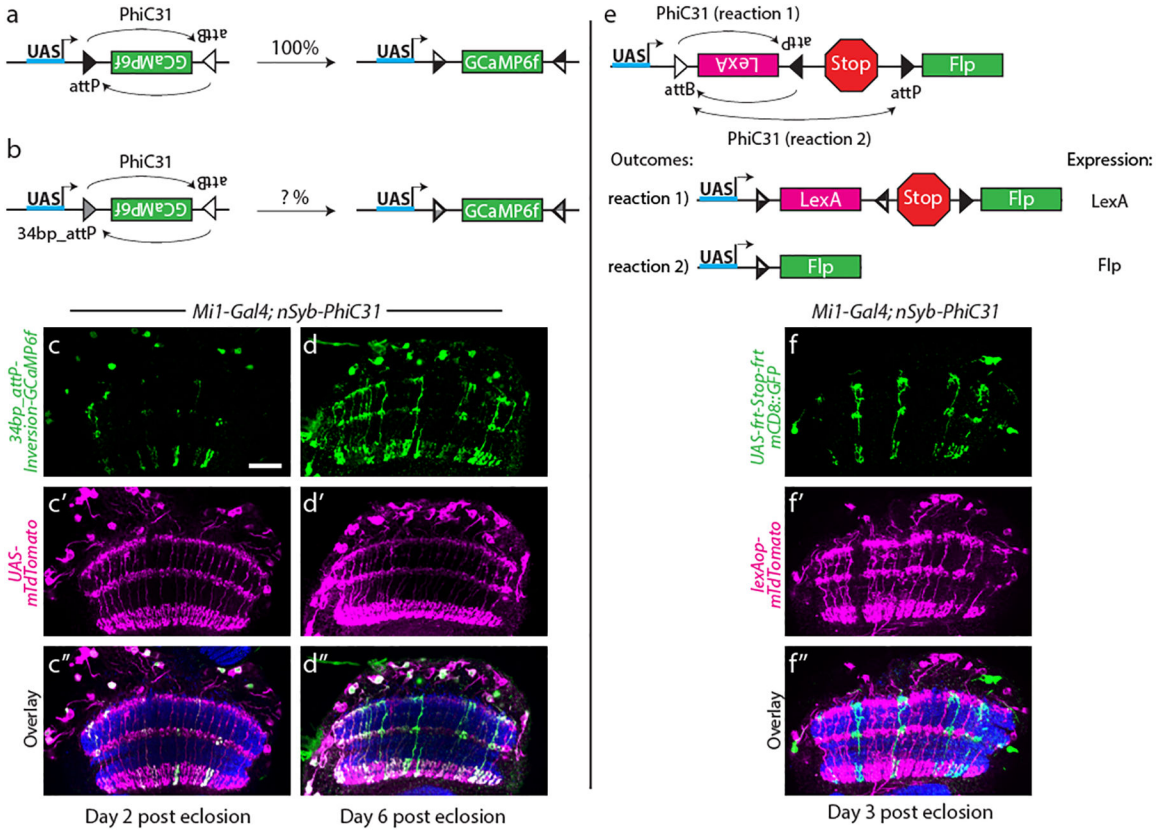

Extended Data Figure 1. SPARC development cassettes.

(a,b) Schematics of PhiC31-dependent *UAS-inversion effector* constructs. (a) control construct with canonical *attP* sites and (b) truncated *34bp_attP* experimental construct. **(c-d")** *34bp_attP*-Inversion-GCaMP6f expression (green, c,d) in Mi1 neurons (magenta, c'-d') counterstained with anti-Bruchpilot (Brp; blue, overlay c"-d"). Fewer Mi1 neurons are labeled at day two post eclosion (c-c") than at day six post eclosion (d-d"). **(e)** Schematic of the LexA-OR-Flp expression construct. PhiC31 recombines one of two competing *attP* target sequences with one *attB* target sequence to enable either LexA or Flp expression. Reaction 1 leads to LexA expression. Reaction 2 leads to Flp expression. **(f-f")** Flp-enabled mCD8::GFP expression (green, f) or LexA-driven myr::tdTomato expression in Mi1 neurons (magenta, f') counterstained with anti-Bruchpilot (Brp; blue, overlay f"). n = 10 optic lobes per genotype. Scale bar: 10μm.

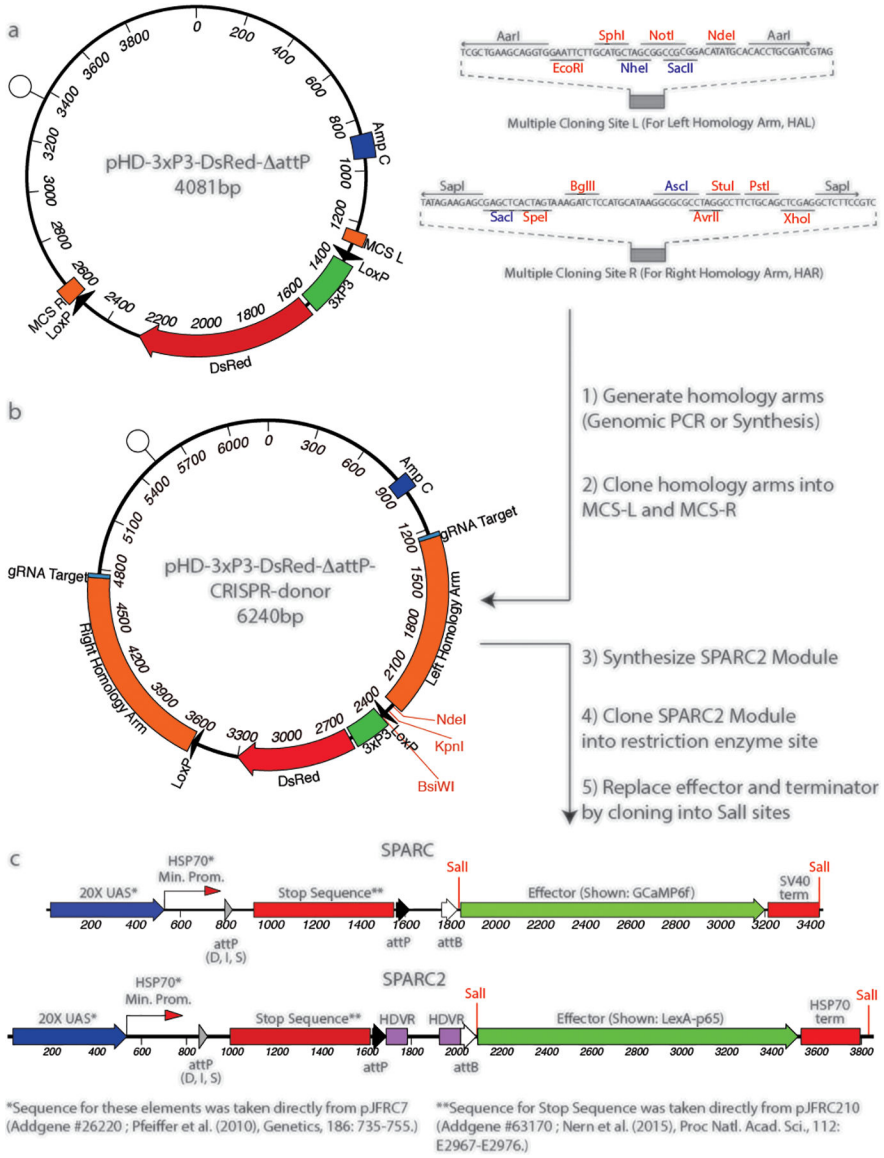

Extended Data Figure 2. Plasmid maps and molecular cloning methods for SPARC and SPARC2 constructs.

(a) Map of pHD-3xP3-DsRed-Δ*attP* (a CRISPR-HDR-donor precursor) showing multiple cloning sites for homology arm insertion (right). **(b)** Map of pHD-3xP3-DsRed-Δ*attP*-CRISPR-donor (example includes homology arms targeting the *attP40* region of the *Drosophila* genome). **(c)** SPARC and SPARC2 cassettes are inserted into pHD-3xP3-DsRed-Δ*attP*-CRISPR-donor via unique KpnI, NdeI, or BsiWI restriction enzyme sites. SalI restriction enzyme sites in the SPARC2 module allow for one-step swapping of the effector and terminator to generate pHD-SPARC2 donor plasmids. Abbreviations: MCS – multiple cloning site; gRNA – guide RNA; HDVR – hepatitis delta virus ribozyme sequence.

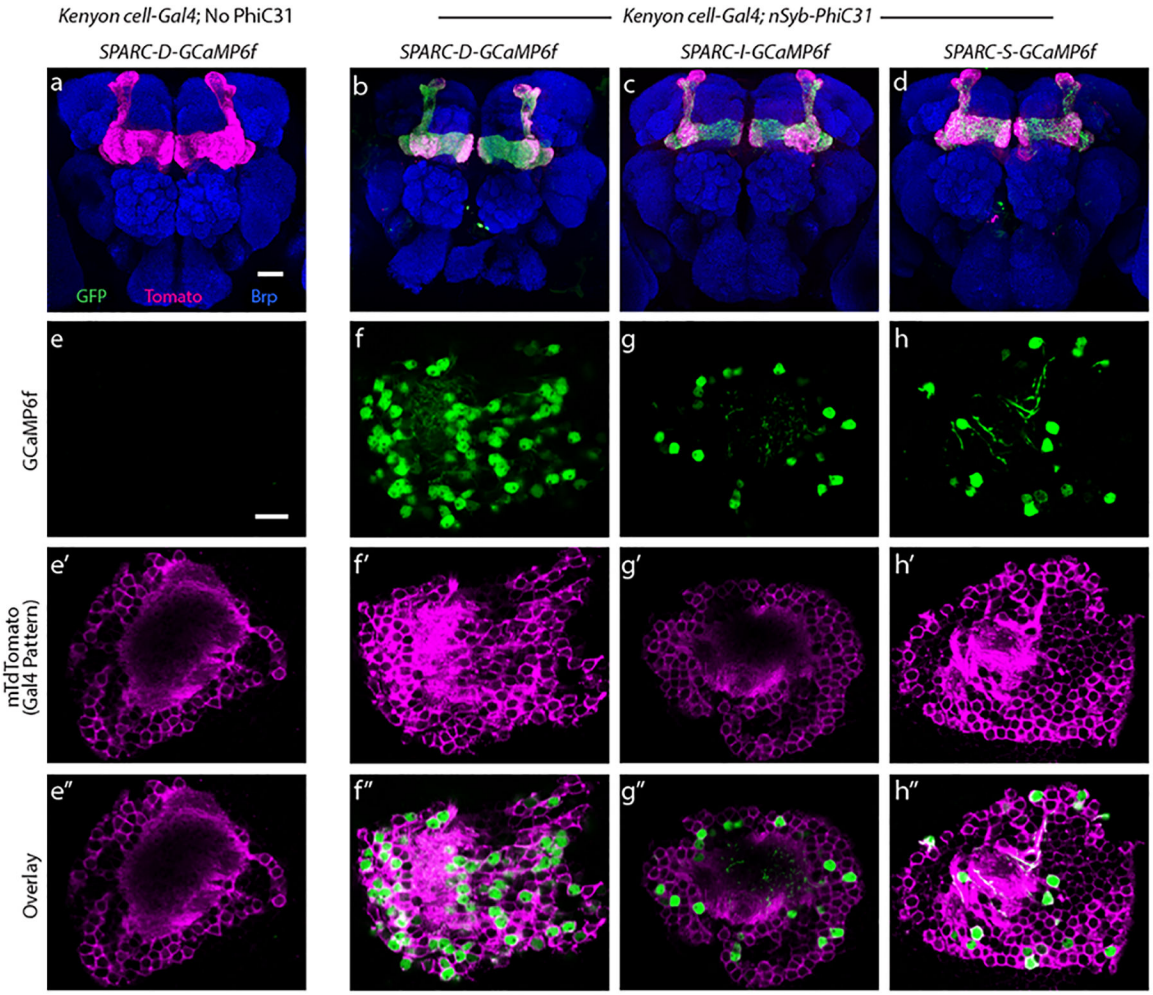

Extended Data Figure 3. SPARC-GCaMP6f expression in Kenyon cells.

(a-d) Anterior view of the *Drosophila* central brain showing GCaMP6f expression (green) in Kenyon cells (magenta) counterstained with anti-Bruchpilot (Brp; blue). (a) *SPARC-D-GCaMP6f*, no PhiC31. (b) *SPARC-D-GCaMP6f*. (c) *SPARC-I-GCaMP6f*. (d) *SPARC-S-GCaMP6f*. **(e-h")** GCaMP6f expression (green, e-h) in Kenyon cell bodies (magenta, e'-h') with overlay (e"-h"). (e-e") *SPARC-D-GCaMP6f*, no PhiC31. GCaMP6f is not detected in Kenyon Cells in the absence of PhiC31. (f-f") *SPARC-D-GCaMP6f*. (g-g") *SPARC-I-GCaMP6f*. (h-h") *SPARC-S-GCaMP6f*. Scale bars: 30μm (a-d), 10μm (e-h"). n > 10 brains per condition from three independent experiments.

SPARC and SPARC2 user guide

a) Important notes:

1. SPARC and SPARC2 activity requires a minimum of three transgenes: 1) *SPARC-effector*, 2) *promoter-PhiC31*, and 3) *enhancer-GAL4*.
2. *SPARC-effector* or *SPARC2-effector* and *promoter-PhiC31* transgenes MUST be maintained in separate stocks. If both transgenes are present in the same fly, there is a possibility that unanticipated PhiC31 expression in the germline will lead to stable recombination of the *SPARC* or *SPARC2* cassette.
3. For all new *SPARC-effector* combinations, we recommend using SPARC2.

b) Example crossing schemes for SPARC or SPARC2

$$\frac{+}{+};\ \underset{(near\ \{attP40\})}{SPARC2\text{-}Effector};\ + \quad X \quad \frac{+}{Y};\ \underset{\{su(Hw)attP5\}}{promoter^{*}\text{-}PhiC31};\ \underset{\{attP2\}}{enhancer\text{-}Gal4} \qquad OR$$

$$\frac{+}{+};\ \underset{(near\ \{attP40\})}{SPARC2\text{-}LexA::p65};\ \underset{(variable)}{lexAop\text{-}effector} \quad X \quad \frac{+}{Y};\ \underset{\{su(Hw)attP5\}}{promoter^{*}\text{-}PhiC31};\ \underset{\{attP2\}}{enhancer\text{-}GAL4}$$

* Available stocks: *20XUAS-PhiC31*, *tub-PhiC31*, and *nSyb-PhiC31*

Using split-Gal4 Drivers:

$$\frac{+}{+};\ \underset{(near\ \{attP40\})}{SPARC2\text{-}effector};\ + \quad X \quad \frac{\underset{\{attp18\}}{promoter^{*}\text{-}PhiC31}}{Y};\ \underset{\{attP40\}}{enhancer\text{-}GAL4AD^{**}};\ \underset{\{attP2\}}{enhancer\text{-}GAL4DBD} \qquad OR$$

$$\frac{+}{+};\ \underset{(near\ \{attP40\})}{SPARC2\text{-}LexA::p65};\ \underset{\{variable\}}{lexAop\text{-}effector} \quad X \quad \frac{\underset{\{attp18\}}{promoter^{*}\text{-}PhiC31}}{Y};\ \underset{\{attP40\}}{enhancer\text{-}GAL4AD};\ \underset{\{attP2\}}{enhancer\text{-}GAL4DBD}$$

* Available stocks: *20XUAS-PhiC31* and *nSyb-PhiC31*.

** Note: Janelia split-Gal4 drivers use the p65ADZp activating domain[21].

Extended Data Figure 4. SPARC and SPARC2 user guide.

(a) Important notes regarding SPARC and SPARC2 use and stock maintenance. **(b)** Example crossing schemes for SPARC or SPARC2 to allow expression of effectors.

Supplementary Material

Refer to Web version on PubMed Central for supplementary material.

Acknowledgements:

We thank members of the Clandinin, Wilson, and Maimon labs for discussion of the project and manuscript. We thank A. Chakravorty for generating the SPARC-jGCaMP7f plasmids and S. Gratz, K. O'Connor-Giles (Brown University), C. Xie, L. Luo (Stanford University), B. Pfeiffer and D. Anderson (CalTech) for providing template plasmids for molecular cloning. We also thank G. Rubin and H. Dionne (Janelia Farms) for sharing split-Gal4 stocks, and N. Perrimon (Harvard University) for sharing Cas9 stocks; additionally, stocks obtained from the Bloomington *Drosophila* Stock Center (NIH P40OD018537) were used in this study. The project was supported by the NIH (R01EY022638 and 5P30EY026877 to T.R.C., 5U19NS104655 to T.R.C. and R.E.W). J.I-B. is an Arnold O. Beckman Postdoctoral Fellow; H.H.Y. is an HHMI fellow of the Jane Coffin Childs Memorial Fund for Medical Research; Y.E.F. is supported by a Hanna H. Grey Fellowship from HHMI; C.F.R.W. is supported by an NSF Graduate Research Fellowship (DGE – 1656518). R.I.W. and G.M. are HHMI investigators.

References:

1. Luo L, Callaway EM & Svoboda K Genetic Dissection of Neural Circuits: A Decade of Progress. Neuron 98, 256–281 (2018). [PubMed: 29673479]
2. Duffy JB GAL4 system in Drosophila: a fly geneticist's Swiss army knife. Genesis 34, 1–15 (2002). [PubMed: 12324939]
3. Golic KG & Lindquist S The FLP recombinase of yeast catalyzes site-specific recombination in the Drosophila genome. Cell 59, 499–509 (1989). [PubMed: 2509077]
4. Sauer B & Henderson N Site-specific DNA recombination in mammalian cells by the Cre recombinase of bacteriophage P1. PNAS 85, 5166–5170 (1988). [PubMed: 2839833]
5. Yeh E, Gustafson K & Boulianne GL Green fluorescent protein as a vital marker and reporter of gene expression in Drosophila. PNAS 92, 7036–7040 (1995). [PubMed: 7624365]
6. Akerboom J et al. Optimization of a GCaMP Calcium Indicator for Neural Activity Imaging. J. Neurosci 32, 13819–13840 (2012). [PubMed: 23035093]
7. Fenno L, Yizhar O & Deisseroth K The Development and Application of Optogenetics. Annu. Rev. Neurosci 34, 389–412 (2011). [PubMed: 21692661]
8. Atasoy D, Aponte Y, Su HH & Sternson SM A FLEX Switch Targets Channelrhodopsin-2 to Multiple Cell Types for Imaging and Long-Range Circuit Mapping. J. Neurosci 28, 7025–7030 (2008). [PubMed: 18614669]
9. Lin R et al. Cell-type-specific and projection-specific brain- wide reconstruction of single neurons. Nat. Methods 1–9 (2018). doi:10.1038/s41592-018-0184-y
10. Feil R et al. Ligand-activated site-specific recombination in mice. PNAS 93, 10887–10890 (1996). [PubMed: 8855277]
11. Livet J et al. Transgenic strategies for combinatorial expression of fluorescent proteins in the nervous system. Nature 450, 56–62 (2007). [PubMed: 17972876]
12. Zong H, Espinosa JS, Su HH, Muzumdar MD & Luo L Mosaic Analysis with Double Markers in Mice. Cell 121, 479–492 (2005). [PubMed: 15882628]
13. Lee T & Luo L Mosaic analysis with a repressible cell marker for studies of gene function in neuronal morphogenesis. Neuron 22, 451–461 (1999). [PubMed: 10197526]
14. Hadjieconomou D et al. Flybow: genetic multicolor cell labeling for neural circuit analysis in Drosophila melanogaster. Nat. Methods 8, 260–266 (2011). [PubMed: 21297619]
15. Hampel S et al. Drosophila Brainbow: a recombinase-based fluorescence labeling technique to subdivide neural expression patterns. Nat. Methods 8, 253–259 (2011). [PubMed: 21297621]
16. Sethi S & Wang JW A versatile genetic tool for post-translational control of gene expression in *Drosophila* melanogaster. eLife 6, e04577 (2017).
17. Gordon MD & Scott K Motor Control in a Drosophila Taste Circuit. Neuron 61, 373–384 (2009). [PubMed: 19217375]
18. Bohm RA et al. A genetic mosaic approach for neural circuit mapping in Drosophila. Proc. Natl. Acad. Sci. U.S.A 107, 16378–16383 (2010). [PubMed: 20810922]
19. Philipsborn, von AC et al. Neuronal Control of Drosophila Courtship Song. Neuron 69, 509–522 (2011). [PubMed: 21315261]
20. Nern A, Pfeiffer BD & Rubin GM Optimized tools for multicolor stochastic labeling reveal diverse stereotyped cell arrangements in the fly visual system. Proc. Natl. Acad. Sci. U.S.A 112, E2967–76 (2015). [PubMed: 25964354]
21. Dionne H, Hibbard KL, Cavallaro A, Kao J-C & Rubin GM Genetic Reagents for Making Split-GAL4 Lines in Drosophila. Genetics 209, 31–35 (2018). [PubMed: 29535151]
22. Jenett A et al. A GAL4-Driver Line Resource for Drosophila Neurobiology. CellReports 2, 991–1001 (2012).
23. Thorpe HM & Smith MC In vitro site-specific integration of bacteriophage DNA catalyzed by a recombinase of the resolvase/invertase family. PNAS 95, 5505–5510 (1998). [PubMed: 9576912]
24. Groth AC, Olivares EC, Thyagarajan B & Calos MP A phage integrase directs efficient site-specific integration in human cells. Proc. Natl. Acad. Sci. U.S.A 97, 5995–6000 (2000). [PubMed: 10801973]

25. Hong W et al. Leucine-rich repeat transmembrane proteins instruct discrete dendrite targeting in an olfactory map. Nat Neurosci 12, 1542–1550 (2009). [PubMed: 19915565]
26. Riabinina O et al. Improved and expanded Q-system reagents for genetic manipulations. Nat. Methods 12, 219–222 (2015). [PubMed: 25581800]
27. Pinto-Teixeira F et al. Development of Concurrent Retinotopic Maps in the Fly Motion Detection Circuit. Cell 1–26 (2018). doi:10.1016/j.cell.2018.02.053
28. Pfeiffer BD et al. Refinement of Tools for Targeted Gene Expression in Drosophila. Genetics 186, 735–755 (2010). [PubMed: 20697123]
29. Lai S-L & Lee T Genetic mosaic with dual binary transcriptional systems in Drosophila. Nat Neurosci 9, 703–709 (2006). [PubMed: 16582903]
30. Perrotta AT & Been MD A pseudoknot-like structure required for efficient self-cleavage of hepatitis delta virus RNA. Nature 350, 434–436 (1991). [PubMed: 2011192]
31. Wernet MF, Klovstad M & Clandinin TR A Drosophila toolkit for the visualization and quantification of viral replication launched from transgenic genomes. PLoS ONE 9, e112092 (2014). [PubMed: 25386852]
32. Schnell B et al. Processing of Horizontal Optic Flow in Three Visual Interneurons of the *Drosophila* Brain. J. Neurophysiol 103, 1646–1657 (2010). [PubMed: 20089816]
33. Sanes JR & Zipursky SL Design principles of insect and vertebrate visual systems. Neuron 66, 15–36 (2010). [PubMed: 20399726]
34. Jefferis GS, Marin EC, Stocker RF & Luo L Target neuron prespecification in the olfactory map of Drosophila. Nature 414, 204–208 (2001). [PubMed: 11719930]
35. Wu M et al. Visual projection neurons in the Drosophila lobula link feature detection to distinct behavioral programs. eLife 5, e21022 (2016). [PubMed: 28029094]
36. Maisak MS et al. A directional tuning map of Drosophila elementary motion detectors. Nature 500, 212–216 (2013). [PubMed: 23925246]
37. Fisher YE, Silies M & Clandinin TR Orientation Selectivity Sharpens Motion Detection in Drosophila. Neuron 88, 390–402 (2015). [PubMed: 26456048]
38. Leong JCS, Esch JJ, Poole B, Ganguli S & Clandinin TR Direction Selectivity in Drosophila Emerges from Preferred-Direction Enhancement and Null-Direction Suppression. Journal of Neuroscience 36, 8078–8092 (2016). [PubMed: 27488629]
39. Wienecke CFR, Leong JCS & Clandinin TR Linear Summation Underlies Direction Selectivity in Drosophila. Neuron 1–14 (2018). doi:10.1016/j.neuron.2018.07.005
40. Klapoetke NC et al. Independent optical excitation of distinct neural populations. Nat. Methods 11, 338–346 (2014). [PubMed: 24509633]
41. Seelig JD & Jayaraman V Feature detection and orientation tuning in the Drosophila central complex. Nature 503, 262–266 (2013). [PubMed: 24107996]
42. Omoto JJ et al. Neuronal constituents and putative interactions within the Drosophila ellipsoid body neuropil 1–49 (2018). doi:10.1101/394833
43. Mosimann C et al. Site-directed zebrafish transgenesis into single landing sites with the phiC31 integrase system. Dev. Dyn 242, 949–963 (2013). [PubMed: 23723152]
44. Olivares EC et al. Site-specific genomic integration produces therapeutic Factor IX levels in mice. Nature Biotechnology 20, 1124–1128 (2002).
45. Fischbach PKF & Dittrich APM The optic lobe of Drosophila melanogaster. I. A Golgi analysis of wild-type structure. Cell Tissue Res 258, 441–475 (1989).
46. Gohl DM et al. A versatile in vivo system for directed dissection of gene expression patterns. Nat. Methods 8, 231–237 (2011). [PubMed: 21473015]
47. Gratz SJ et al. Highly specific and efficient CRISPR/Cas9-catalyzed homology-directed repair in Drosophila. Genetics 196, 961–971 (2014). [PubMed: 24478335]
48. Silies M et al. Modular use of peripheral input channels tunes motion-detecting circuitry. Neuron 79, 111–127 (2013). [PubMed: 23849199]
49. Housden BE et al. Identification of potential drug targets for tuberous sclerosis complex by synthetic screens combining CRISPR-based knockouts with RNAi. Sci Signal 8, rs9–rs9 (2015). [PubMed: 26350902]

50. Wilson RI, Turner GC & Laurent G Transformation of olfactory representations in the Drosophila antennal lobe. Science 303, 366–370 (2004). [PubMed: 14684826]

51. Schindelin J et al. Fiji: an open-source platform for biological-image analysis. Nature Publishing Group 9, 676–682 (2012).

52. Leonhardt A et al. Asymmetry of Drosophila ON and OFF motion detectors enhances real-world velocity estimation. Nat Neurosci 19, 706–715 (2016). [PubMed: 26928063]

53. Pnevmatikakis EA et al. Simultaneous Denoising, Deconvolution, and Demixing of Calcium Imaging Data. Neuron 89, 285–299 (2016). [PubMed: 26774160]

54. Fişek M & Wilson RI Stereotyped connectivity and computations in higher-order olfactory neurons. Nat Neurosci 17, 280–288 (2014). [PubMed: 24362761]

55. Gouwens NW & Wilson RI Signal propagation in Drosophila central neurons. Journal of Neuroscience 29, 6239–6249 (2009). [PubMed: 19439602]

56. Nern A, Pfeiffer BD & Rubin GM Optimized tools for multicolor stochastic labeling reveal diverse stereotyped cell arrangements in the fly visual system. Proc. Natl. Acad. Sci. U.S.A 112, E2967–76 (2015). [PubMed: 25964354]

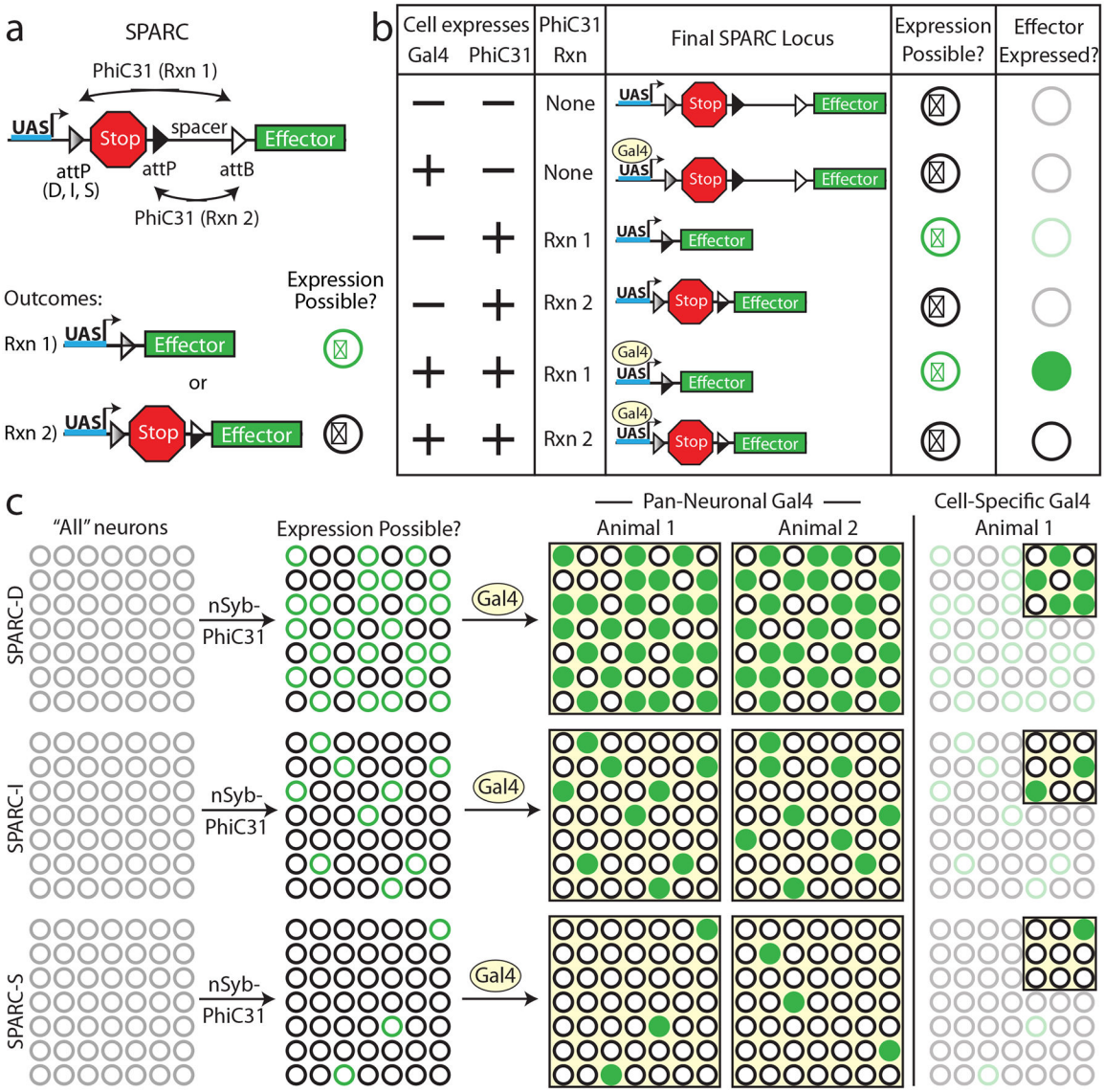

Figure 1: Schematic description of the SPARC method.

(a) Schematic of the SPARC cassette. PhiC31 recombines one of two competing *attP* target sequences with one *attB* target sequence. Progressively truncating the first *attP* favors retention of the stop cassette, preventing expression of effector (Dense (D): 60bp, canonical sequence; Intermediate (I): 38bp; Sparse (S): 34bp). Rxn 1 describes the cassette rearrangement that produces effector expression. Rxn 2 describes the cassette rearrangement that fails to produce effector expression. **(b)** Table illustrating how PhiC31 and Gal4 expression in a cell can impact the SPARC cassette and SPARC effector expression. Effector expression occurs only in cells that express both PhiC31 and Gal4 and in which Rxn 1 occurs. **(c)** Schematic of SPARC effector expression in cell populations. PhiC31 expressed from *nSyb-PhiC31* recombines the SPARC cassettes in all cells, rendering Gal4/UAS expression of the effector possible (Rxn 1; open green circle) or not possible (Rxn 2; open black circle) in three predictable proportions depending on the sequence of the first *attP* in the SPARC cassette (D, I, S). Gal4 is expressed in either all of these neurons (Pan-Neuronal

Gal4) or a subset of these neurons (Cell-Specific Gal4) but can only drive effector expression (closed green circle) in the stochastic subset of cells in which SPARC Rxn 1 has occurred. Because the SPARC reaction is stochastic, different animals (Animal 1, Animal 2) will express effector in different subsets of cells within the Gal4 pattern.

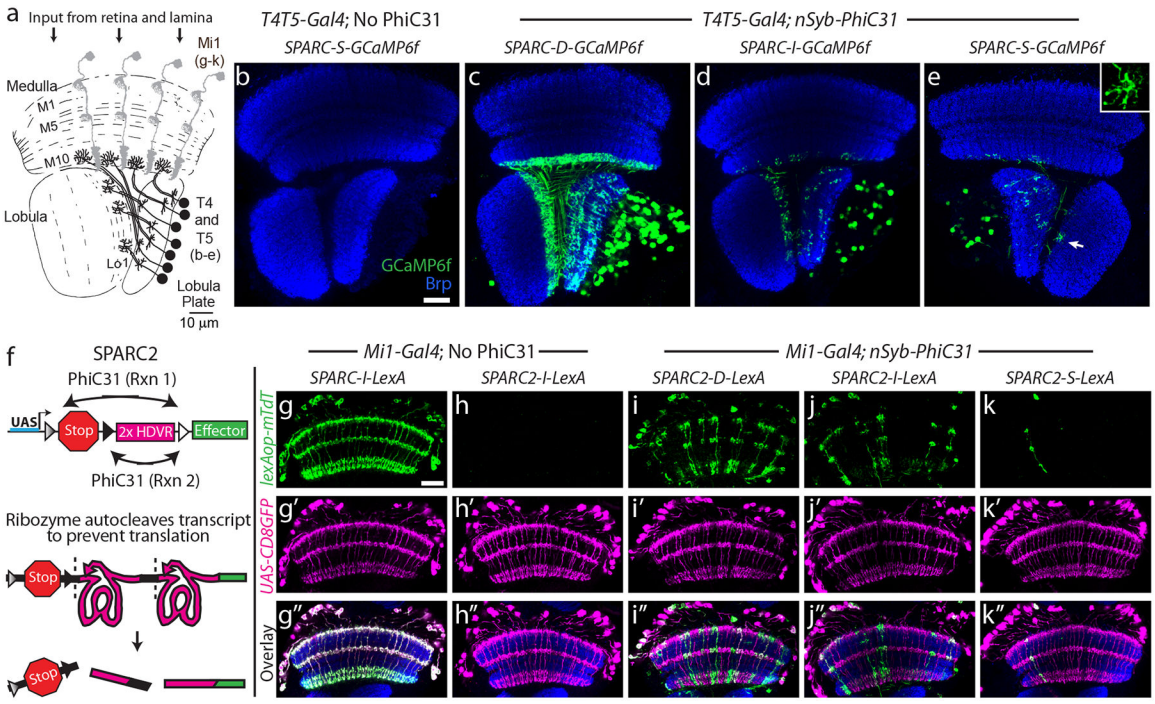

Figure 2: The SPARC toolkit enables predictable expression of effectors at three levels.

(a) Schematic of the *Drosophila* optic lobe highlighting T4, T5, and Mi1[45]. **(b-e)** GCaMP6f expression (green) in T4 and T5 neurons counterstained with anti-Bruchpilot (Brp, synaptic protein; blue). (b) *SPARC-S-GCaMP6f*, no PhiC31. (c) *SPARC-D-GCaMP6f*. (d) *SPARC-I-GCaMP6f*. (e) *SPARC-S-GCaMP6f*, arrow points to dendrite shown in inset. n > 10 optic lobes per genotype, observed in three independent experiments. **(f)** Schematic of the SPARC2 cassette including the 2X hepatitis delta virus ribozyme (HDVR) sequence. **(g-k)** LexA::p65-driven expression of myr::tdTomato (green, g-k), in Mi1 neurons (magenta, g'-k') counterstained with anti-Bruchpilot (Brp; blue, overlay, g"-k"). (g) *SPARC-I-LexA::p65*, no PhiC31. (h) *SPARC2-I-LexA::p65*, no PhiC31. (i) *SPARC2-D-LexA::p65*. (j) *SPARC2-I-LexA::p65*. (k) *SPARC2-S-LexA::p65*. Scale bars: 10µm. n > 10 optic lobes per condition, observed in three independent experiments.

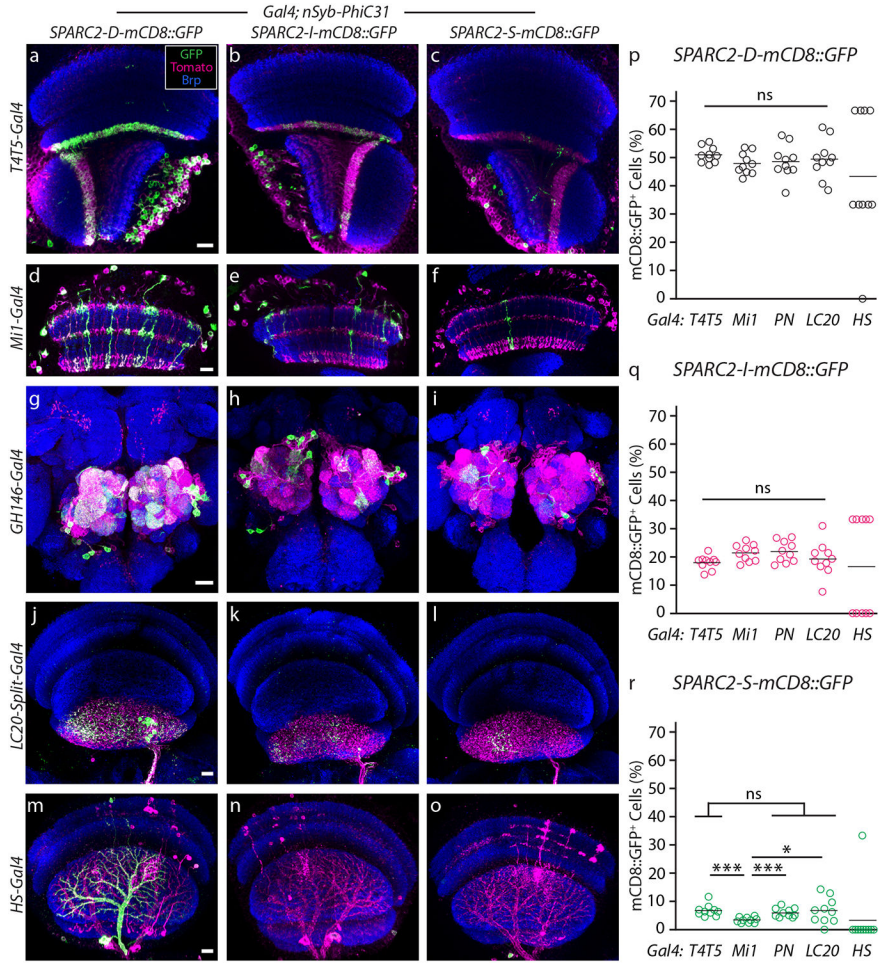

Figure 3: SPARC2 labels precise proportions of neurons across a diverse set of cell types.

(a-o) SPARC2-mCD8::GFP expression (green) in different neuron populations (magenta) counterstained with anti-Bruchpilot (Brp; blue). SPARC2-D-mCD8::GFP, SPARC2-I-mCD8::GFP, and SPARC2-S-mCD8::GFP in the following cell types (a-c) T4 and T5 neurons, (d-f) Mi1 neurons, (g-i) olfactory projection neurons (PNs) in the *GH146-Gal4+* population, (j-l) LC20 neurons, and (m-o) HS neurons. **(p-r)** Percentage of neurons labeled by different SPARC2 modules. (p) SPARC2-D-mCD8::GFP (black circles). (q) SPARC2-I-mCD8::GFP (magenta circles). (r) SPARC2-S-mCD8::GFP (green circles). n = 10 optic lobes or antenna lobes per genotype, from two independent experiments; bars indicate mean value. Scale bars: 10μm (a-i) or 15μm (j-o). ns = not significant (1-way ANOVA); * = p = 0.03 (Mi1 vs. LC20) and *** p = 0.0002 (Mi1 vs. T4T5) or p = 0.0003 (Mi1 vs. PN; two-sided Student's t-test). Within a cell type, all differences between D, I, and S variants are statistically significant ($p<0.0001$, two-sided Student's t-test). We excluded HS from statistical analyses (see \ Methods).

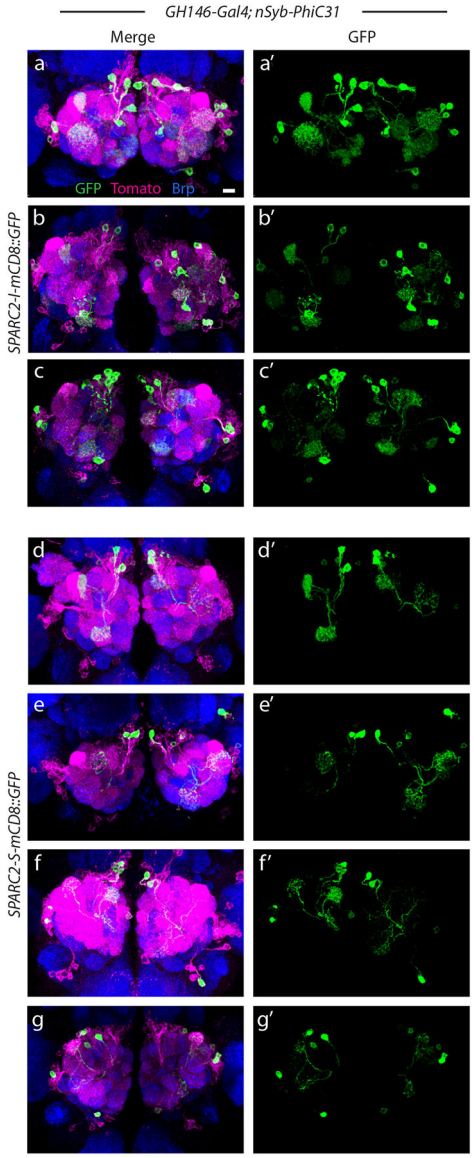

Figure 4: SPARC2 stochastically labels different subsets of neurons in each animal.

(a-g) SPARC2-mCD8::GFP expression (green) in olfactory PNs targeted by *GH146-Gal4* (magenta; myr::tdTomato reporter) counterstained with anti-Bruchpilot (Brp; blue). (a-c') *SPARC2-I-mCD8::GFP* and (d-g') *SPARC2-S-mCD8::GFP*. 7 brains shown, representative of n = 10 brains per genotype. Scale bar: 10μm.

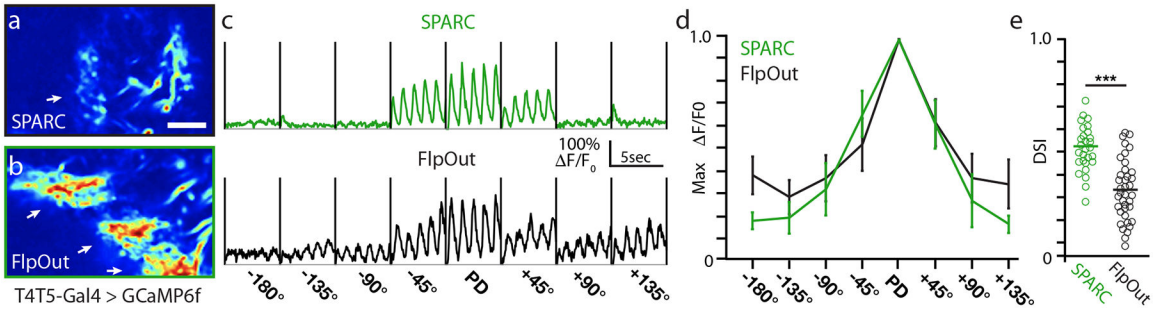

Figure 5: SPARC enables calcium imaging of single neurons.

(a,b) Normalized averaged fluorescence intensity of GCaMP6f in T5 dendrites sparsely labeled using (a) *SPARC-S-GCaMP6f* or (b) *FlpOut-Gal80*-enabled expression. Arrows point to dendrites. n = 8 experiments **(c,d)** GCaMP6f fluorescence responses ($\Delta F/F_0$) of T5 dendritic ROIs to sinusoidal gratings moving in one of eight different directions. PD denotes the preferred direction of each cell with the angular deviation from PD in degrees (c) Averaged responses of a representative ROI expressing GCaMP6f using *SPARC-S-GCaMP6f* (green) or *FlpOut-Gal80*-enabled expression (black). n = 8 experiments (d) Normalized tuning curves averaged across all T5 dendritic ROIs. n = 8 flies and 37 units per condition, center values indicate means, error bars show one standard deviation from the mean. **(e)** Direction-selectivity indices (DSI) for each T5 dendritic ROI. n = 8 flies and 37 units per condition; ***p = 3.75E-10 (two-tailed Student's t-test), bars represent the mean. Scale bar: 10μm.

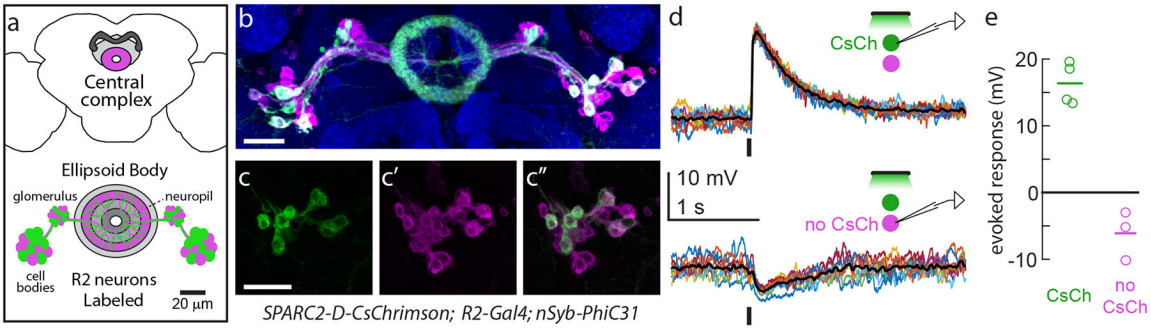

Figure 6: SPARC2 enables optogenetic stimulation of sparse cell populations.

(a) Schematic of the central complex and ellipsoid body depicting SPARC2-labeled R2 ring neurons. **(b)** SPARC2-D-CsChrimson::tdTomato-3.1 expression (tdTomato; green) in R2 neurons (mCD8::GFP; magenta) counterstained with anti-Bruchpilot (Brp; blue). Image is representative of five individual brains stained from two independent experiments **(c-c")** Closeup of cell bodies on the right in (b) showing (c) CsChrimson expression in (c') R2 cells. (c") Overlay. **(d)** Current-clamp recordings of single tdTomato^{+} (top) and tdTomato^{-} (bottom) R2 neurons. Stimulus is a 50-ms pulse of green light (vertical bar); 10 trials each (colored lines), mean response (black line). (e) Average evoked response (open circles) and mean population response (line) of R2 neurons, both tdTomato^{+} (green, n = 4) and tdTomato^{-} (magenta, n = 3); each neural recording (d,e) was an independent experiment. Scale bars: 20μm.